Computers & Geosciences 159 (2022) 104948

Contents lists available at ScienceDirect

Computers and Geosciences

journal homepage: www.elsevier.com/locate/cageo

Research paper

A framework for automatically choosing the optimal parameters of finite-difference scheme in the acoustic wave modeling

Guiting Chen [a,b], Zhenming Peng [a,b,*], Yalin Li [c,*]

[a] School of Information and Communication Engineering, University of Electronic Science and Technology of China, No. 4, Section 2, North Jianshe Road, Chengdu, Postal Code: 610054, China

[b] Laboratory of Imaging Detection and Intelligent Perception, University of Electronic Science and Technology of China, Chengdu, Postal Code: 610054, China

[c] PetroChina Tarim Oilfield Company, Korla, Xinjiang, Postal Code: 841000, China

ARTICLE INFO

Keywords:
Finite-difference scheme
FD parameters
Dispersion relationship
Stability condition
Inhomogeneous model

ABSTRACT

An effective finite-difference (FD) scheme requires suitable FD parameters to ensure stability while having sufficient accuracy in the seismic modeling. The FD parameters such as time step, grid spacing and FD operator also affect the computational costs and storage requirements significantly. Thus, choosing the FD parameters should be the optimal trade-off between the stability, numerical accuracy and computational efficiency. However, the FD parameters usually be chosen through repeated manual tests, which is prone to unnecessary consumption. In this paper, we propose a framework for automatically choosing the FD parameters to achieve the optimal FD scheme in the acoustic wave modeling. Considering the computational efficiency, the proposed framework provides the maximum admissible time step under the stability condition. On the premise of the maximum time step, the proposed framework can find suitable parameters to ensure that the FD scheme has sufficient wavenumber bandwidth to deal with the maximum wavenumber or frequency of the wavefield. Dispersion and stability analyses prove that the FD parameters determined by our framework can effectively avoid dispersion errors while ensuring stability under the given conditions. Numerical experiments also prove the effectiveness of the framework in choosing FD parameters for the inhomogeneous velocity model. The framework can easily obtain the optimal FD parameters and can be recommended as a routine step for the FD methods.

1. Introduction

Finite-difference (FD) method is a powerful tool for solving the seismic wave equation due to its simplicity and high efficiency (Dablain, 1986; Etgen and O' Brien, 2007; Virieux et al., 2011; Liu and Sen, 2011; Moczo et al., 2011, 2014; Le et al., 2020; Fang et al., 2020), and the FD method has evolved into an essential step of the advanced seismic imaging and velocity modeling techniques, such as the reverse time migration (McMechan, 1983; Liu et al., 2013) and full waveform inversion (Virieux and Operto, 2009; Pan et al., 2020). However, the explicit FD schemes do not necessarily provide accurate solutions to the wave equation. Besides, FD schemes have to adhere to strict requirements to ensure that the simulation is stable. The parameters of the FD scheme such as time step, grid spacing, FD operator and velocity are like a knob to adjust the numerical accuracy and stability. However, as far as we know, how to choose the optimal parameters to balance the accuracy, stability and computational efficiency has not been sufficiently investigated.

A von Neumann stability analysis (Neumann, 1932; Mufti, 1990; Wu et al., 1996; Lines et al., 1999; Chu et al., 2009; Chen, 2011) can be used to show that the stability factor should be greater than that of the Courant number, otherwise the FD scheme is unstable (Liu and Sen, 2009). Where the Courant number is related to the FD parameters. The stability factor is related to the weighted sum of the FD coefficients (Finkelstein and Kastner, 2007; Liu and Sen, 2009, 2011). For the case of inhomogeneous velocity model, the FD method partitions the velocity model into nodes that lie on the regular or irregular grid, each node may contain a different value for the medium velocity. To ensure that all grid nodes satisfy the stability condition, the stability factor should be greater than the Courant number corresponding to the maximum velocity of the model. Generally, increasing maximum velocity requires decreasing the time step or increasing the grid spacing (Moczo et al., 2000; Amundsen and Pedersen, 2017; Gao et al., 2018). However, too small time step increases the computational cost considerably, while a large grid spacing is prone to the dispersion

* Corresponding authors.
E-mail addresses: zmpeng@uestc.edu.cn (Z. Peng), liyal_sc@cnpc.com.cn (Y. Li).

https://doi.org/10.1016/j.cageo.2021.104948
Received 23 November 2020; Received in revised form 16 September 2021; Accepted 21 September 2021
Available online 15 November 2021

errors. Besides, choosing time step or other FD parameters is a nonlinear problem, where changing one value (e.g., time step) will changes the optimal choice for other parameters.

According to the Nyquist sampling theorem, a wavefield must be sampled at two grid-points per minimum wavelength in order to avoid aliasing. This requirement also applies to the wavefield modeled with the FD method: the grid nodes must be placed close-enough to each other to make sure that all wavenumbers of the modeled wavefield are sampled accurately. That is, the maximum wavenumber of wavefield cannot exceed the Nyquist wavenumber, otherwise there will be aliasing. However, a large grid spacing easily makes the maximum wavenumber of wavefield larger than the Nyquist wavenumber (Mufti, 1990). In addition, the FD method approximates the derivatives in the continuous wave equation is inaccurate. The errors generally get worse for higher wavenumbers, which are propagated at erroneous velocities, a process referred to as numerical dispersion (Liu and Sen, 2011). The dispersion relation equation (Dablain, 1986) is usually used to analyze the dispersion error of the FD scheme, and the wavenumber range satisfying the dispersion relation equation is called the wavenumber bandwidth. To avoid the dispersion error, the wavenumber bandwidth should include the maximum wavenumber of the wavefield (Zhang and Yao, 2012; Liu, 2013). Dispersion analyses show that decreasing grid spacing can significantly increase the wavenumber bandwidth (Liu and Sen, 2011), so as to mitigate the numerical dispersion. However, a small grid spacing is easy to make the FD scheme unstable in the high-velocity part of the model, especially for the model with strong velocity contrast. For a small grid spacing, we should also choose a small time step to ensure the stability, but the computational burden is greatly increased. Therefore, an appropriate grid spacing not only ensure that the FD scheme is free from numerical dispersion and stability problem, but also avoid unnecessary computational cost.

FD parameters usually be chosen through repeated manual tests. However, the manual tests hardly obtain the optimal solution due to there is no quantitative analyses of the dispersion error and stability. In this paper, we propose a framework to automatically choose the optimal FD parameters to avoid unnecessary computational cost while ensuring sufficient accuracy. For any given velocity model, the proposed framework chooses the FD parameters according to the dispersion relationship and stability condition. Dispersion and stability analyses prove that the proposed framework not only ensure that the maximum expected wavenumber in the wavefield is accurately modeled, but also ensure that the FD parameters will not be chosen any smaller than required. Numerical experiments also prove that the proposed framework provides great convenience for seismic modeling in the inhomogeneous velocity model.

2. Method

In this paper, the second-order scalar wave equation with a regular-grid FD scheme is used as an example to introduce the framework. The first-order system with the 2-D or 3-D staggered-grid FD schemes can be applied to this framework in the same way. In addition, the framework uses the well-known time–space domain method to obtain the FD coefficients (Liu and Sen, 2011). For other methods, we only need to modify the corresponding dispersion and stability formulas.

2.1. Dispersion relation for the wave equation

The 2-D scalar acoustic equation for space (x, z) and time t with a constant density and velocity v can be written as

$$\frac{1}{v^2}\frac{\partial^2 p}{\partial t^2} = \frac{\partial^2 p}{\partial x^2} + \frac{\partial^2 p}{\partial z^2}, \tag{1}$$

where $p(x, z, t)$ represents the scalar wavefield. We assume a plane-wave solution for $p(x, z, t) = p_0 e^{i(k_x x + k_z z - \omega t)}$, where the wavenumbers $k_x = k\cos(\theta)$ and $k_z = k\sin(\theta)$. Then substitution in Eq. (1) gives

$$\frac{1}{v^2}(-i\omega)^2 = (ik_x)^2 + (ik_z)^2, \tag{2}$$

providing the well-known dispersion relation

$$|v| = \frac{\omega}{|\sqrt{k_x^2 + k_z^2}|} = \frac{\omega}{|\mathbf{k}|}, \tag{3}$$

for vector $\mathbf{k} = (k_x, k_z)^T$.

2.2. Defining the FD operators

Now we introduce the central FD approximations for the derivative operators:

$$\frac{\partial^2 p}{\partial t^2} \approx \frac{\delta^2 p}{\delta t^2} = \frac{1}{\tau^2}\left[-2p_{0,0}^0 + \left(p_{0,0}^{-1} + p_{0,0}^1\right)\right], \tag{4}$$

$$\frac{\partial^2 p}{\partial x^2} \approx \frac{\delta^2 p}{\delta x^2} = \frac{1}{h^2}\left[a_0 p_{0,0}^0 + \sum_{m=1}^{M} a_m\left(p_{-m,0}^0 + p_{m,0}^0\right)\right], \tag{5}$$

and

$$\frac{\partial^2 p}{\partial z^2} \approx \frac{\delta^2 p}{\delta z^2} = \frac{1}{h^2}\left[a_0 p_{0,0}^0 + \sum_{m=1}^{M} a_m\left(p_{0,-m}^0 + p_{0,m}^0\right)\right]. \tag{6}$$

Here, we use a shorthand notation $p_{m,n}^l = p(x + mh, z + nh, t + l\tau)$ for the grid spacing h and time step τ. The FD coefficients a_m should be chosen such that the (M)-th order accurate FD approximations are accurate. Substituting (4), (5) and (6) into Eq. (1), we obtain the FD equation

$$\begin{aligned}\frac{1}{h^2}&\left[2a_0 p_{0,0}^0 + \sum_{m=1}^{M} a_m\left(p_{-m,0}^0 + p_{m,0}^0 + p_{0,-m}^0 + p_{0,m}^0\right)\right] \\ &\approx \frac{1}{v^2\tau^2}\left[-2p_{0,0}^0 + \left(p_{0,0}^{-1} + p_{0,0}^1\right)\right].\end{aligned} \tag{7}$$

Assuming the plane waves propagate in the grid for $p_{m,n}^l = p_0 e^{i[k_x(x+mh)+k_z(z+nh)-\omega(t+l\tau)]}$, these approximations lead to the following behavior

$$a_0 + \sum_{m=1}^{M} a_m\left[\cos(mk_x h) + \cos(mk_z h)\right] \approx r^{-2}\left[-1 + \cos(\omega\tau)\right]. \tag{8}$$

Here, $r = v\tau/h$ represents the Courant number. We follow the Taylor expansion method from Liu and Sen (2009) (equation 32 in their paper), which transforms Eq. (8) into

$$\begin{cases} a_0 + 2\sum_{m=1}^{M} a_m = 0 \\ \sum_{m=1}^{M} m^{2j}\left(\cos^{2j}\theta + \sin^{2j}\theta\right) a_m = r^{2j-2} \qquad (j = 1, 2, \ldots, M). \end{cases} \tag{9}$$

Eq. (9) represents the well-known time–space domain method for solving the FD coefficients. For any θ, we can expand Eq. (9) into a linear system and obtain the FD coefficients by numerical methods. The time–space domain FD coefficients are related to the Courant number. Here, we define a new symbol r_a, which specifically represents the Courant number used to determine the FD coefficients a_{m,r_a}. To mitigate the spatial dispersion errors, $r_a = v_{min}\tau/h$ corresponding to the minimum velocity is usually used.

2.3. Dispersion analyses for the FD equations

Using the dispersion relation in Eq. (8), we find

$$\omega = \frac{1}{\tau}\arccos\left\{1 + r^2\left[\sum_{m=1}^{M} a_{m,r_a}\left(\cos(mk_x h) + \cos(mk_z h) - 2\right)\right]\right\}. \tag{10}$$

We can write down the phase velocity $v_{FD} = \omega/|\mathbf{k}|$ produced in the FD scheme by dividing Eq. (10) by $|\mathbf{k}|$. Dividing the resulting expression by v then yields the phase velocity error ratio

$$\delta(r_a, r, \alpha, \beta) = \frac{v_{FD}}{v}$$

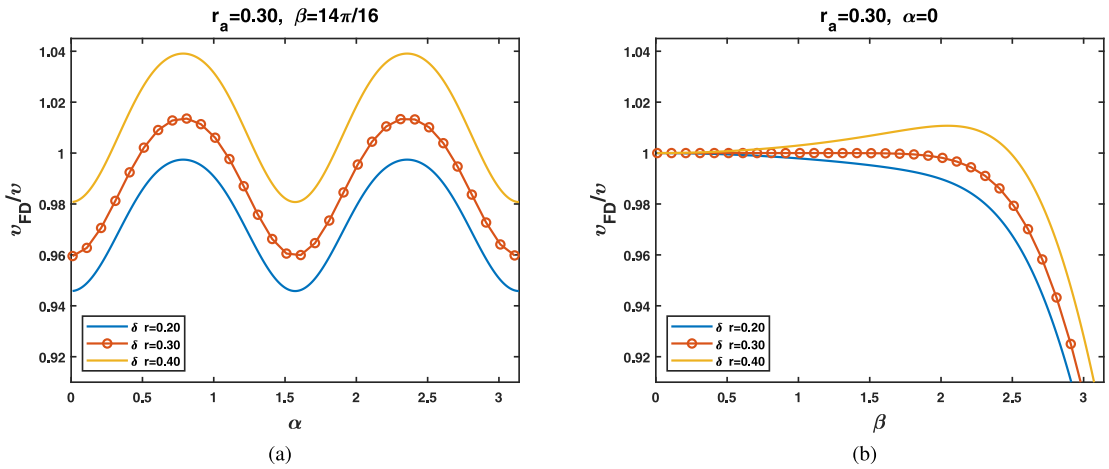

Fig. 1. Dispersion curves with different Courant numbers r. Here we set a fixed $r_a = 0.30$ to determine FD coefficients and analyze their dispersion curves with different Courant number r. (a) represents the dispersion curves varying with the propagation angle α. (b) represents the dispersion curves varying with the parameter β.

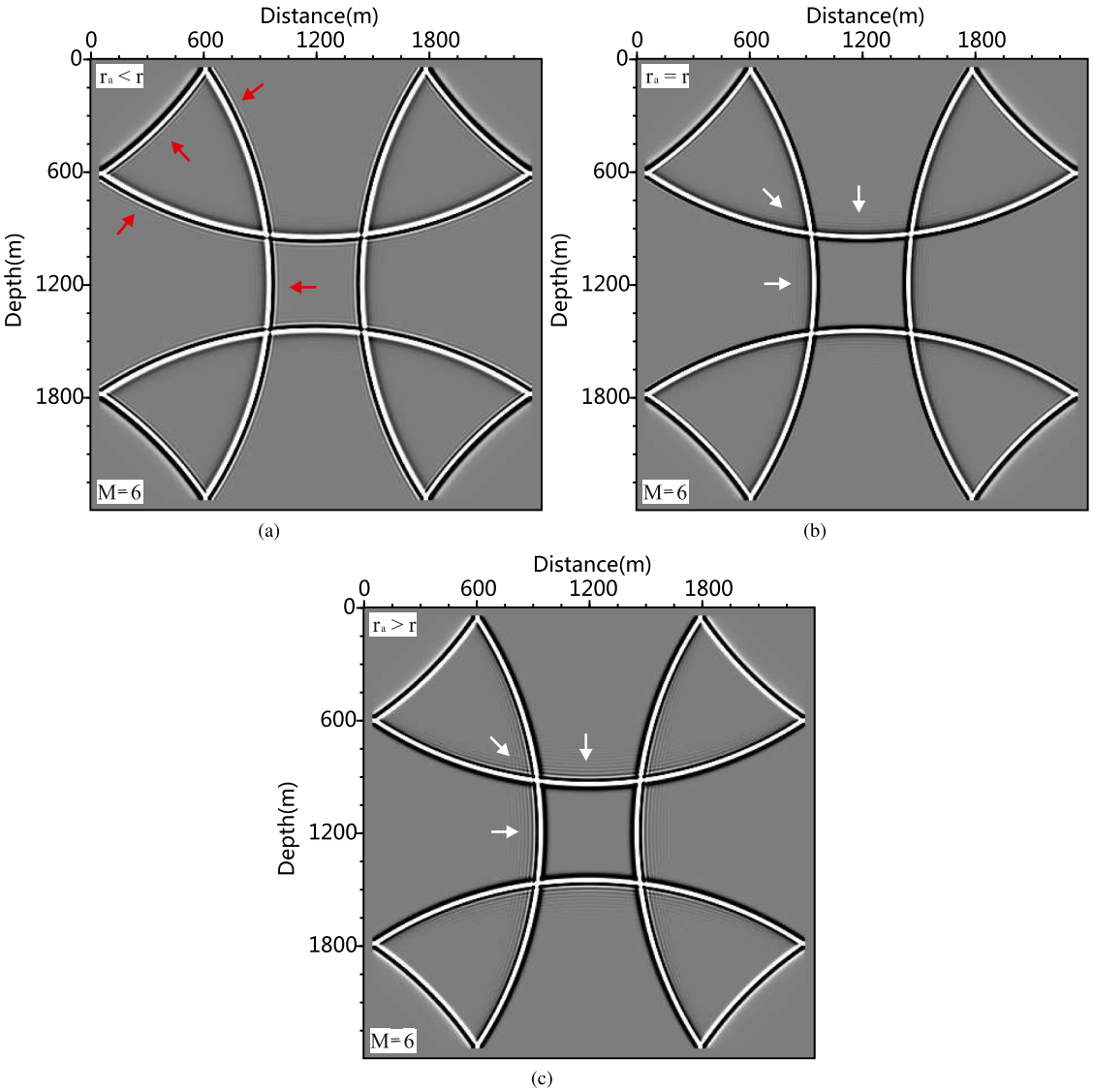

Fig. 2. Snapshots with different Courant numbers r. (a) represents the case of $r_a < r$; (b) represents the case of $r_a = r$. (c) represents the case of $r_a > r$.

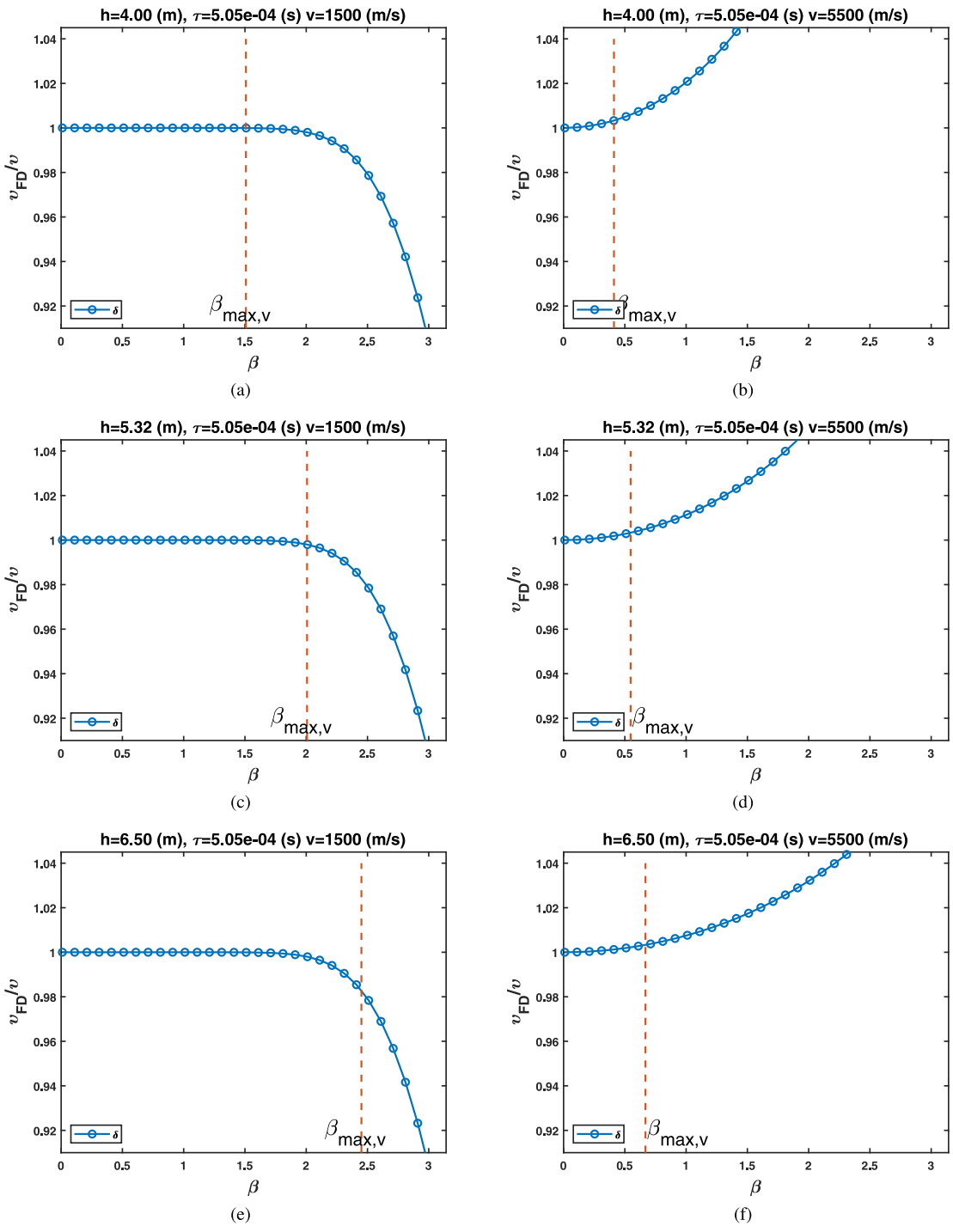

Fig. 3. Dispersion curves of the cases in Table 1. Here we set $r_a = v_{min}\tau/h$ and analyze their dispersion curves with different grid spacings. The left panel shows the dispersion curves with a low velocity ($v = 1500$ m/s), and the right panel shows the dispersion curves with a high velocity ($v = 5500$ m/s). (a) and (b) represent the case of $h = 4.00$ m. (c) and (d) represent the case of $h = 5.32$ m. (e) and (f) represent the case of $h = 6.50$ m.

$$= \frac{1}{r\beta}\arccos\left[1 + r^2\left(\sum_{m=1}^{M} a_{m,r_a}\left(\cos(m\beta\cos\alpha) + \cos(m\beta\sin\alpha) - 2\right)\right)\right]. \tag{11}$$

Here, we use a specialized symbol α instead of θ to represent the propagation angle for dispersion analysis, and $\beta = kh$. If $\delta(r_a, r, \alpha, \beta)$ equals 1, the FD scheme propagates waves at the correct numerical velocity. If not, the FD scheme contains numerical dispersion, i.e., has the spatial dispersion error ($\delta(r_a, r, \alpha, \beta) < 1$) or temporal dispersion error ($\delta(r_a, r, \alpha, \beta) > 1$). To analyze the numerical dispersion under different Courant numbers r_a and r, we design a series of FD parameters and show their dispersion curves and corresponding wavefield snapshots. The dispersion curves of the $\delta(r_a, r, \alpha, \beta)$ varying with the parameter β are shown in Fig. 1 and the wavefield snapshots are shown in Fig. 2.

As shown in Fig. 1, the FD schemes have obvious spatial dispersion errors ($r_a > r$) and temporal dispersion errors ($r_a < r$). Only when $r_a = r$, the FD scheme has a relatively good dispersion curve. The same conclusion can be also found in the numerical simulation. As shown in Fig. 2, the snapshot of the case $r_a < r$ has obvious temporal dispersion errors (red arrows), and the case $r_a > r$ is prone to spatial dispersion

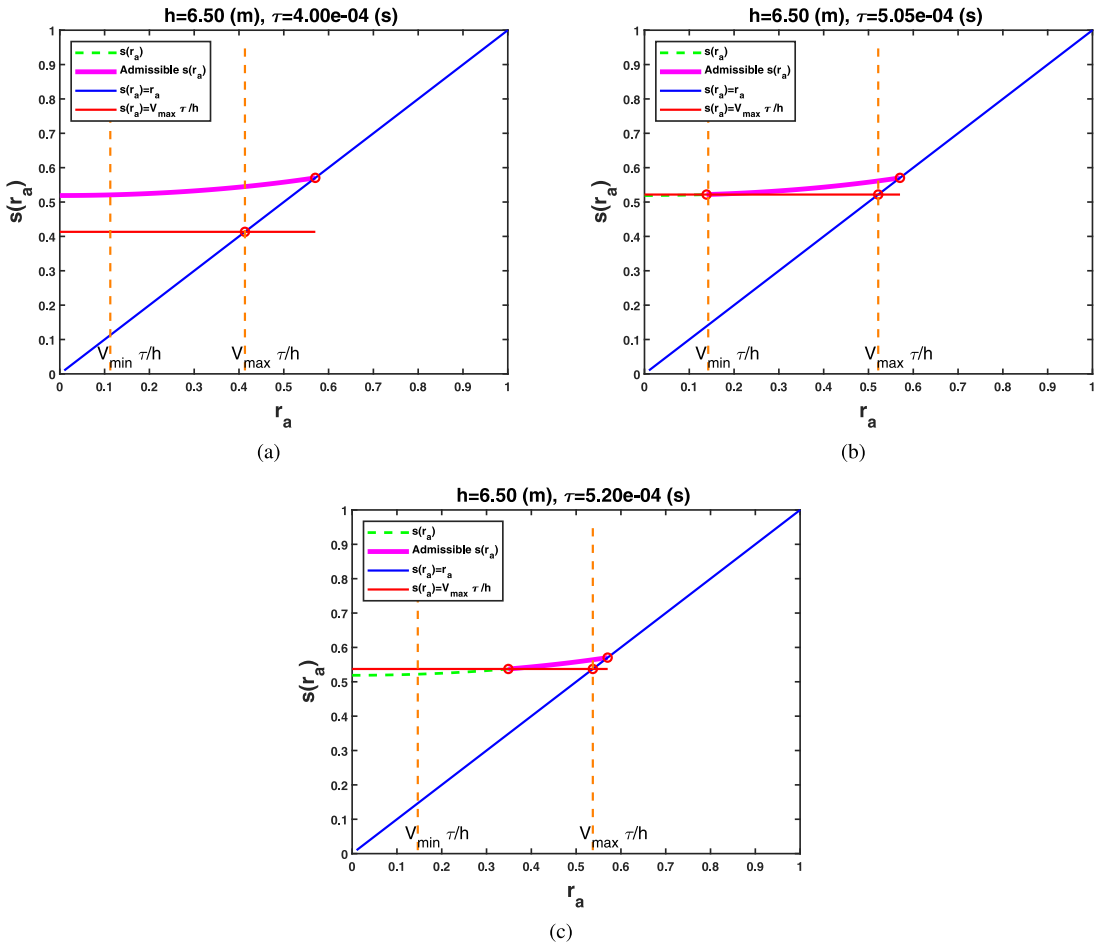

Fig. 4. Stability curves with different time steps τ. Here the green curves represent the stability factor $s(r_a)$, the pink curves represent the admissible range of r_a and the red curves represent $v_{max}\tau/h$ corresponding the maximum velocity. Obviously, the admissible range (pink curve) must be above the red curve. (a) represents the stability curve with a small time step τ. (b) represents a middle time step and (c) represents a large time step. (For interpretation of the references to color in this figure legend, the reader is referred to the web version of this article.)

Table 1
FD dispersion error of different FD parameters. Here we set $M = 8$, $f_{max} = 30 * 3$ Hz, $v_{min} = 1500$ m/s and $v_{max} = 5500$ m/s for all cases.

Cases	h (m)	τ (s)	$\left\|\delta(r_a, r_{min}, \alpha, \beta_{max,v_{min}}) - 1\right\|$	$\left\|\delta(r_a, r_{max}, \alpha, \beta_{max,v_{max}}) - 1\right\|$	ξ
1	4.00	5.05e−04	5.12e−05	3.17e−03	3.22e−03
2	5.32	5.05e−04	1.97e−03	3.17e−03	5.14e−03
3	6.50	5.05e−04	1.71e−02	3.17e−03	2.03e−02

errors(white arrows). Dispersion analyses and numerical simulations reveal that the Courant number r_a should be equal to r as much as possible. However, for an inhomogeneous velocity model, the Courant number r varies with the medium velocity of the grid node. The courant number r_a for determining FD coefficients cannot always be equal to r.

2.4. Choice of FD parameters

2.4.1. Choice of grid spacing h: prevent aliasing and dispersion

The grid spacing h must ensure that the solution is at least not aliased. A solution is not aliased when wavenumbers in our plane-wave solution are sampled according to $|\mathbf{k}| \le |\mathbf{k_N}|$, where we use $|\mathbf{k}|$ from Eq. (3) and the Nyquist wavenumber $|\mathbf{k_N}| = \pi/h$. Rewriting this inequality, we find

$$h \le \frac{v\pi}{\omega} = \frac{v\pi}{2\pi f} = \frac{v}{2f}, \tag{12}$$

where f is the frequency of the corresponding plane wave solution. For the case of inhomogeneous model (i.e., a varying velocity $v(x, z)$) with all frequencies, we must choose h according to the most restrictive conditions

$$h \le \frac{v_{min}}{2f_{max}}. \tag{13}$$

Here, v_{min} represents the minimum velocity in the modeling domain, and f_{max} represents the maximum frequency of wavefield. Thus, the maximum value of grid spacing is $h_{max} = v_{min}/(2f_{max})$, otherwise the solution is aliased.

Considering the numerical dispersion, the wavenumber bandwidth of FD scheme should at least satisfy the maximum wavenumber $k_{max,v} = 2\pi f_{max}/v$ of the wavefield, and the maximum $\beta_{max,v} = 2\pi f_{max}h/v$ is related to the medium velocity v and maximum frequency f_{max}. For the inhomogeneous velocity model, the velocities of all grid nodes should satisfy their corresponding maximum wavenumbers, we define a criterion to describe the FD dispersion error, i.e.,

$$\xi(h, \tau, v_{min}, v_{max}) = \left|\delta(r_a, r_{min}, \alpha, \beta_{max,v_{min}}) - 1\right| + \left|\delta(r_a, r_{max}, \alpha, \beta_{max,v_{max}}) - 1\right|. \tag{14}$$

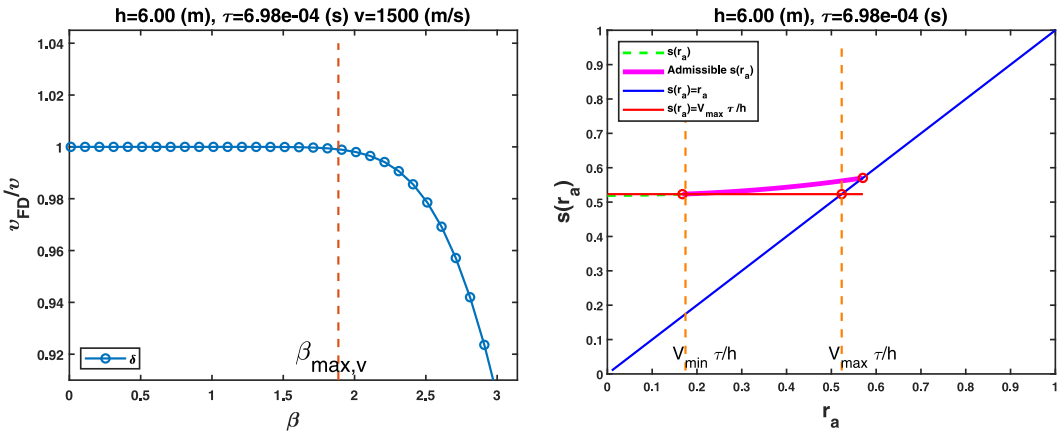

Fig. 5. Dispersion and stability curves of the case 1 in Table 2, where the FD parameters $M = 8$, $f_{max} = 25 * 3$ Hz, $v_{min} = 1500$ m/s, $v_{max} = 4500$ m/s, $h = 6.03$ m and $\tau = 7.01e{-}04$ s. (a) represents the dispersion curve. (b) represents the stability curve.

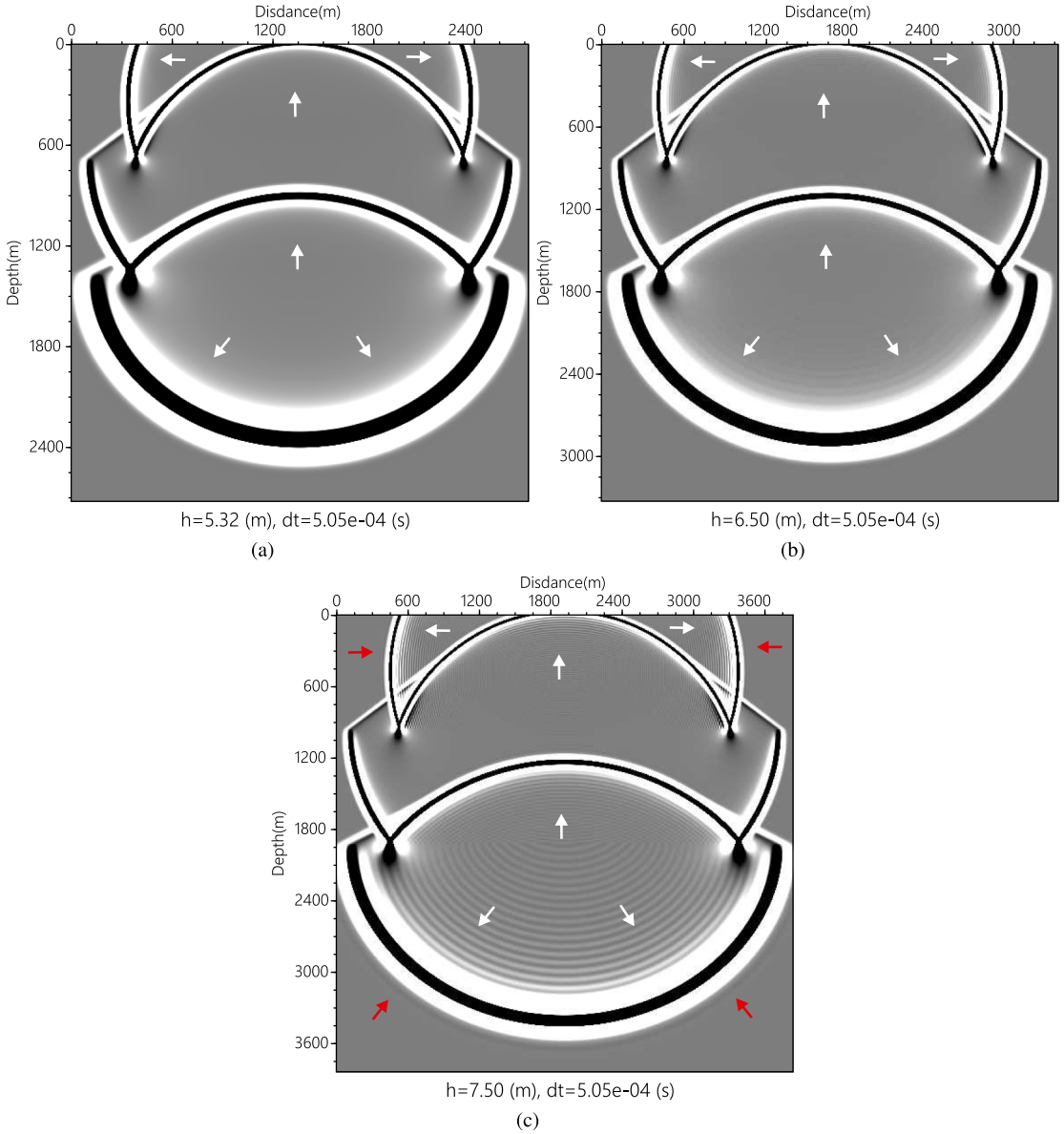

Fig. 6. Snapshots of the 2-D model with different grid spacings h in Table 3. (a) $h = 5.32$ m, (b) $h = 6.50$ m. (c) $h = 7.50$ m.

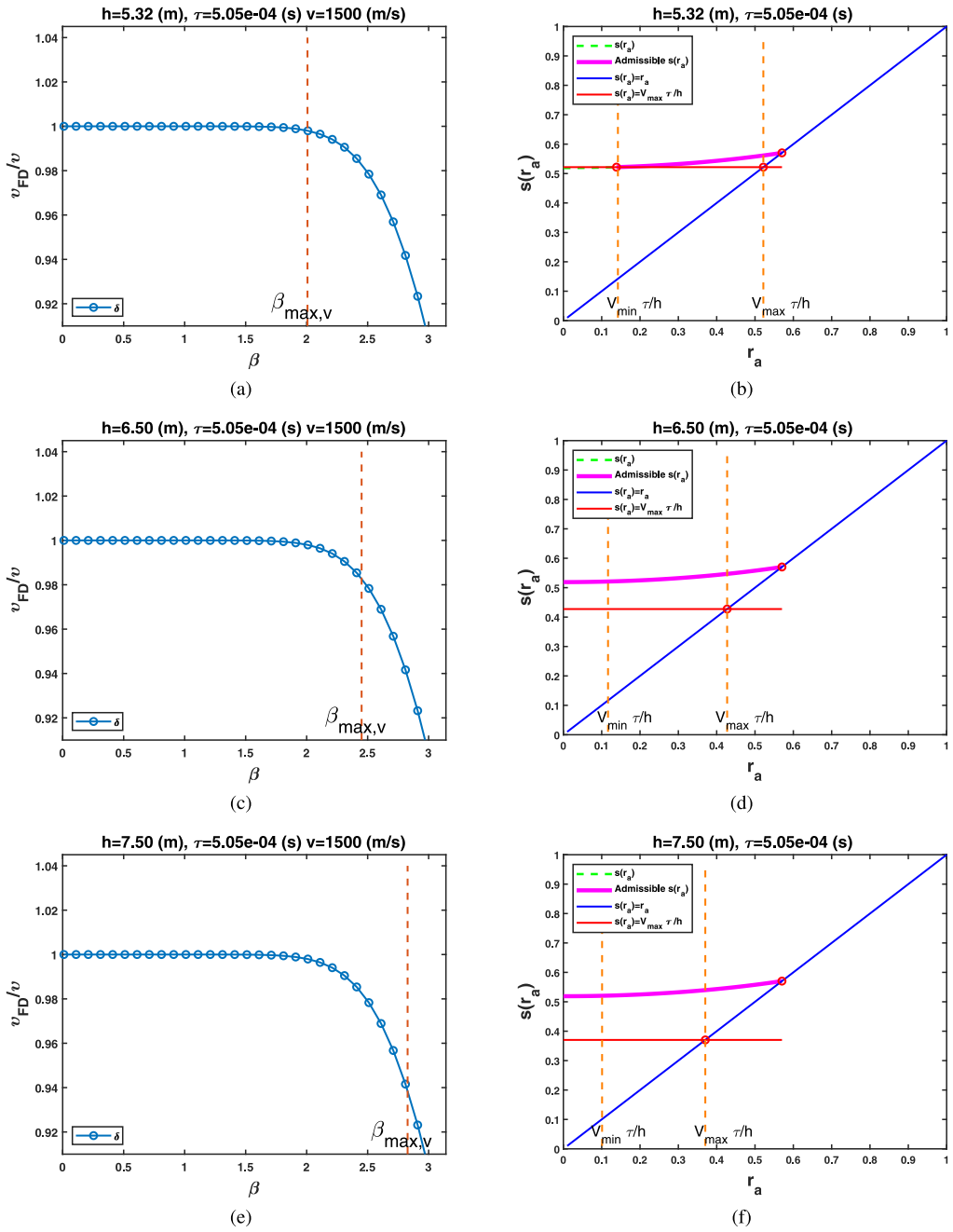

Fig. 7. Dispersion and stability curves for different grid spacings h in Table 3. (a) and (b) represent the dispersion and stability curves of $h = 5.32$ m. (c) and (d) represent $h = 6.50$ m. (e) and (f) represent $h = 7.50$ m.

In which $r_{min} = v_{min}\tau/h$, $r_{max} = v_{max}\tau/h$, and $r_a = v_{min}\tau/h$. Considering the minimum dispersion parameter $\delta(r_a, r, \alpha, \beta)_{min} = \delta(r_a, r, n\pi/2, \beta)$, we recommended $\alpha = 0$ for mitigating spatial dispersion errors. In Eq. (14), the first term measures the spatial dispersion error at low-velocity part of the model, and the second term measures the temporal dispersion error at high-velocity part. To analyze the FD dispersion errors with different grid spacings, we design a series of cases and show the $\xi(h, \tau, v_{min}, v_{max})$ in Table 1, and the corresponding dispersion curves are shown in Fig. 3.

As shown in Table 1, the FD dispersion error of the Case 1 ($h = 4.00$ m) is smaller than other cases, and the wavenumber bandwidth has obvious redundancy for the maximum wavenumber of velocity $v_{min} = 1500$ m/s (Fig. 3(a)), which indicates that $h = 4.00$ m is not an economic solution. The FD dispersion error of the Case 3 ($h = 6.50$ m) has increased considerably compared to other cases, and the wavenumber bandwidth of $h = 6.50$ m does not satisfy the maximum wavenumber of velocity $v_{min} = 1500$ m/s (Fig. 3(e)), resulting in numerical dispersion. Fig. 3(c) shows that the case $h = 5.32$ m satisfies the maximum wavenumber without redundancy, and the FD dispersion error ($\xi = 5.14e{-}03$) is acceptable. Therefore, the FD dispersion error defined by Eq. (14) can be used to analyze whether grid spacing is appropriate. We can design a threshold based on our requirements. If $\xi(h, \tau, v_{min}, v_{max})$ is less than the preset threshold, the grid spacing is considered appropriate and the FD scheme has sufficient wavenumber bandwidth to deal with the maximum wavenumber of the wavefield. If not, large dispersion will occur from the high-wavenumber components of the wavefield.

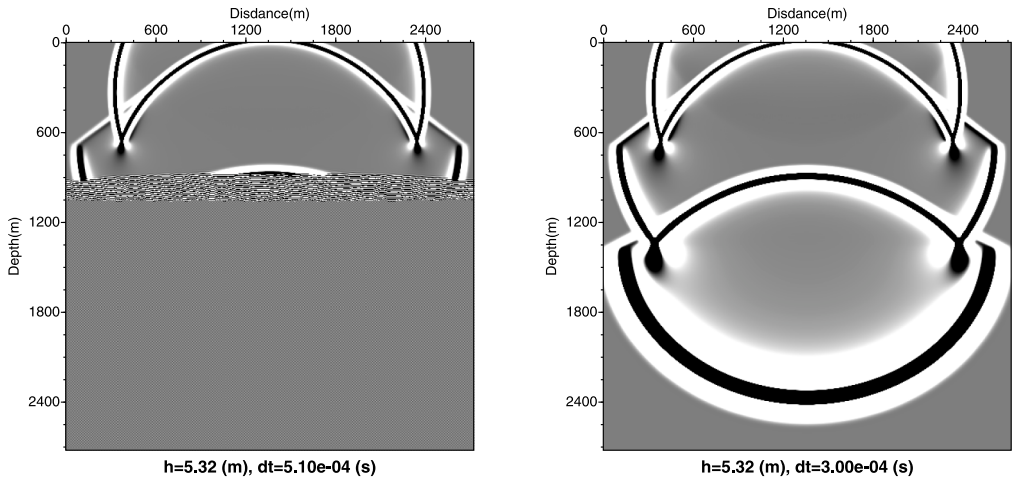

(a) (b)

Fig. 8. Snapshots of the 2-D model with different time steps τ in Table 4. (a) $\tau = 5.10e{-}04$ s and (b) $\tau = 3.00e{-}04$ s.

2.4.2. Choice of time step τ: prevent instability

We derive the stability condition by the well-known von Neumann analyses (Mufti, 1990; Wu et al., 1996; Lines et al., 1999; Moczo et al., 2000; Chen, 2011; Liu and Sen, 2009, 2013). The arccosine function in Eq. (10) requires a real value, so the argument of cosine must lie in the interval $[-1, 1]$. We can thus write

$$\left|1 + r^2 \left[\sum_{m=1}^{M} a_{m,r_a}(\cos(mk_x h) + \cos(mk_z h) - 2)\right]\right| \leq 1. \tag{15}$$

The expression is trivially true for $k_x = k_z = 0$ with any r. Usually, considering the Nyquist wavenumber $k_x = k_z = \pi/h$, we may find

$$-1 \leq 1 + r^2 \left[2\sum_{m=1}^{M} a_{m,r_a}((-1)^m - 1)\right] \leq 1. \tag{16}$$

Rearranging Eq. (16) can obtain the 2-D stability condition

$$\left[\sum_{m=1}^{M} a_{m,r_a}\left((-1)^{m+1} + 1\right)\right]^{-1/2} \geq r. \tag{17}$$

The left-hand side of the inequality (17) is defined as the stability factor

$$s(r_a) = \left[\sum_{m=1}^{M} a_{m,r_a}\left((-1)^{m+1} + 1\right)\right]^{-1/2}, \tag{18}$$

and the 2-D stability condition can be rewritten as

$$s(r_a) \geq r. \tag{19}$$

The FD scheme runs stably only when the stability factor $s(r_a)$ is greater than r. For the inhomogeneous model, the FD scheme should ensure that all velocities satisfy the stability condition, that is

$$s(r_a) \geq \frac{v_{max}\tau}{h}. \tag{20}$$

In Eq. (20) gives the admissible range of r_a for determining the FD coefficients, which strictly guarantees the stability of FD scheme in the inhomogeneous velocity model. In the following, we set different time steps τ with a fixed h to analyze their stability curves according to the in Eq. (20).

As shown in Fig. 4, the pink curves represent the admissible range of r_a. When we set a small time step ($\tau = 4.00e{-}04s$), the admissible $s(r_a)$ is significantly larger than $v_{max}\tau/h$ (Fig. 4(a)), which reveals that $\tau = 4.00e{-}04s$ has redundancy in the stability condition. When we set a large $\tau = 5.20e{-}04s$, the admissible range does not include the Courant number $r_a = v_{min}\tau/h$. However, the FD coefficients determined by the Courant number $r_a = v_{min}\tau/h$ can effectively avoid the spatial dispersion error. Therefore, considering the numerical dispersion, the optimal τ should ensure that the stability factor satisfies

$$s\left(\frac{v_{min}\tau}{h}\right) = \frac{v_{max}\tau}{h}. \tag{21}$$

Eq. (21) ensures that the FD scheme is stable for all grid nodes when $r_a = v_{min}\tau/h$ is used to determine the FD coefficients. The stability curve with the time step $\tau = 5.05e{-}04s$ satisfying Eq. (21) is shown in Fig. 4(b). It can be seen that the admissible range just contains the Courant number $r_a = v_{min}\tau/h$. Thus, Eq. (21) provides the maximum time step when we $r_a = v_{min}\tau/h$ to determine the FD coefficients.

2.4.3. Choice of M: high-enough for accuracy, not higher

The parameter M sets the (half-)size of the FD stencil in each Cartesian direction. It is well-known in FD modeling that increasing M results in more accurate results. If we add more terms to the FD operator, the approximation of the trigonometric function can be made better and better. In this study, we will keep M fixed for the entire simulation but we note that various works exist where M varies along with the velocity model (Liu and Sen, 2011; Liu, 2019).

2.4.4. A framework for choosing the optimal FD parameters

Putting all strategies together, we propose a framework for choosing the optimal parameters. The steps of our framework are:

1. Give the maximum frequency f_{max}, minimum velocity v_{min} and maximum velocity v_{max}.
2. Initialize M, dispersion threshold ξ_τ and stability threshold ξ_h, increment $\delta\tau$ and δh as desired.
3. Estimate an appropriate value for h as follows.

(i) Initialize $h^0 = \frac{V_{min}}{2f_{max}}$ based on the aliasing criterium. Set $i = 0$.

(ii) Estimate the optimal time step τ based on the stability condition for h^i as follows.

(a) Set a very small time step τ^0. Set $j = 0$.
(b) Compute the stability factor $s(\frac{V_{min}\tau^j}{h^i})$.
(c) Check $\left|s(\frac{V_{min}\tau^j}{h^i}) - \frac{V_{max}\tau^j}{h^i}\right| > \xi_\tau$ with the chosen h^i and τ^j.
(d) If the inequality is satisfied, increase $\tau^{j+1} = \tau^j + \delta\tau$, increase j, and repeat this inner loop. If the inequality is not satisfied, exit the loop with τ^{j-1} as the final stable value for τ.

(iii) Compute the FD dispersion error $\xi(h^i, \tau, v_{min}, v_{max})$ with the chosen h^i and corresponding τ.

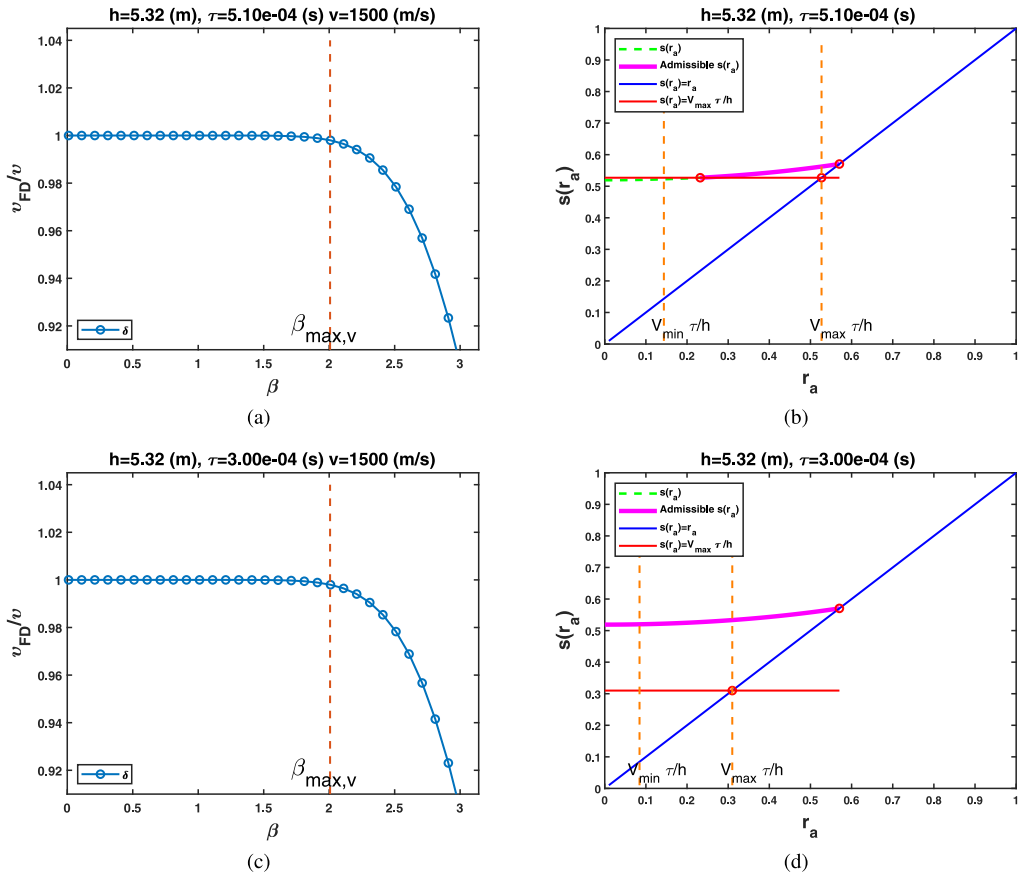

Fig. 9. Dispersion and stability curves for different time steps τ in Table 4. (a) and (b) represent the dispersion and stability curves of $\tau = 5.10e{-}04$ s. (c) and (d) represent $\tau = 3.00e{-}04$ s.

Table 2
Automatically calculated FD parameters h and τ through the proposed framework with different M, f_{max}, v_{min}, v_{max}, ξ_h and ξ_τ. Here, we set dispersion threshold $\xi_h = 0.005$ and stability threshold $\xi_\tau = 0.0002$ for all cases.

Cases	M	f_{max} (Hz)	V_{min} (m/s)	V_{max} (m/s)	h (m)	τ (s)
1	8	$25 * 3$	1500	4500	6.00	$6.98e{-}04$
2	6	$25 * 3$	1500	4500	5.53	$6.58e{-}04$
3	4	$25 * 3$	1500	4500	4.93	$6.12e{-}04$
4	8	$30 * 3$	1500	4500	5.00	$5.81e{-}04$
5	8	$35 * 3$	1500	4500	4.28	$4.98e{-}04$
6	8	$25 * 3$	2000	4500	8.26	$9.68e{-}04$
7	8	$25 * 3$	2500	4500	11.60	$1.00e{-}03$
8	8	$25 * 3$	1500	5000	6.21	$6.48e{-}04$
9	8	$25 * 3$	1500	5500	6.35	$6.02e{-}04$

(iv) Check $\xi(h^i, \tau, v_{min}, v_{max}) > \xi_h$.

(v) If the inequality is satisfied, decrease $h^{i+1} = h^i - \delta h$, increase i, and repeat this inner loop. If the inequality is not satisfied, exit the loop with h^{i-1} as the final stable value for h.

4. Carry out the modeling program using the previously found inputs.

The framework fixes h^i to find the corresponding optimal time step τ, then checks whether the grid spacing h^i is the optimal solution through the FD dispersion error $\xi(h^i, \tau, v_{min}, v_{max})$. If the FD dispersion error $\xi(h^i, \tau, v_{min}, v_{max})$ is less than the preset threshold ξ_h, the optimal FD parameters are found. Otherwise, the framework sets $h^{i+1} = h^i - \delta h$ to continue searching. To verify the feasibility of proposed framework, we design a series of cases and use the proposed framework to obtain the FD parameters automatically, then we also analyze the corresponding dispersion and stability curves. The details of these cases are listed in Table 2.

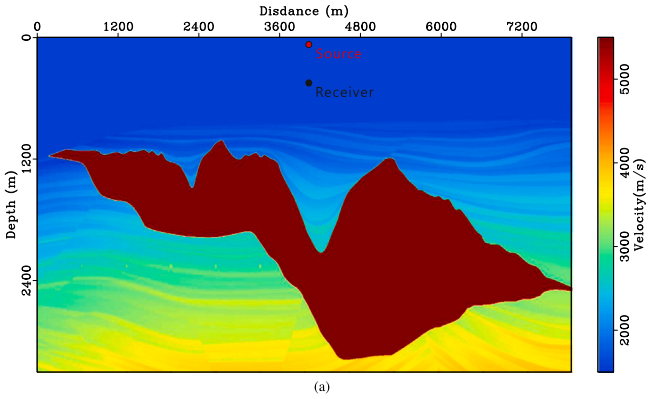

Fig. 10. 2-D Sigsbee model with the velocities from $v_{min} = 1500$ m/s to $v_{max} = 5500$ m/s.

Fig. 5 shows the dispersion and stability curves of the Case 1 in Table 2. It can be seen that the wavenumber bandwidth satisfies the maximum wavenumber and the stability is not redundant. The analyses of Case 1 proves the feasibility of the proposed framework in choosing FD parameters. When M decreases or f_{max} increases (Cases 1 to 5 in Table 2), h and τ are reduced to ensure that the wavenumber bandwidths satisfy the maximum wavenumbers, which is consistent with our experience in the manual testing. The minimum velocity v_{min} has a significant impact on the wavenumber bandwidth. If v_{min} is increased, larger FD parameters can be chosen (Cases 6 and 7). The maximum velocity v_{max} easily leads to instability of the FD scheme. Table 2 confirms that increasing v_{max} requires decreasing τ to ensure stability (Cases 8 and 9).

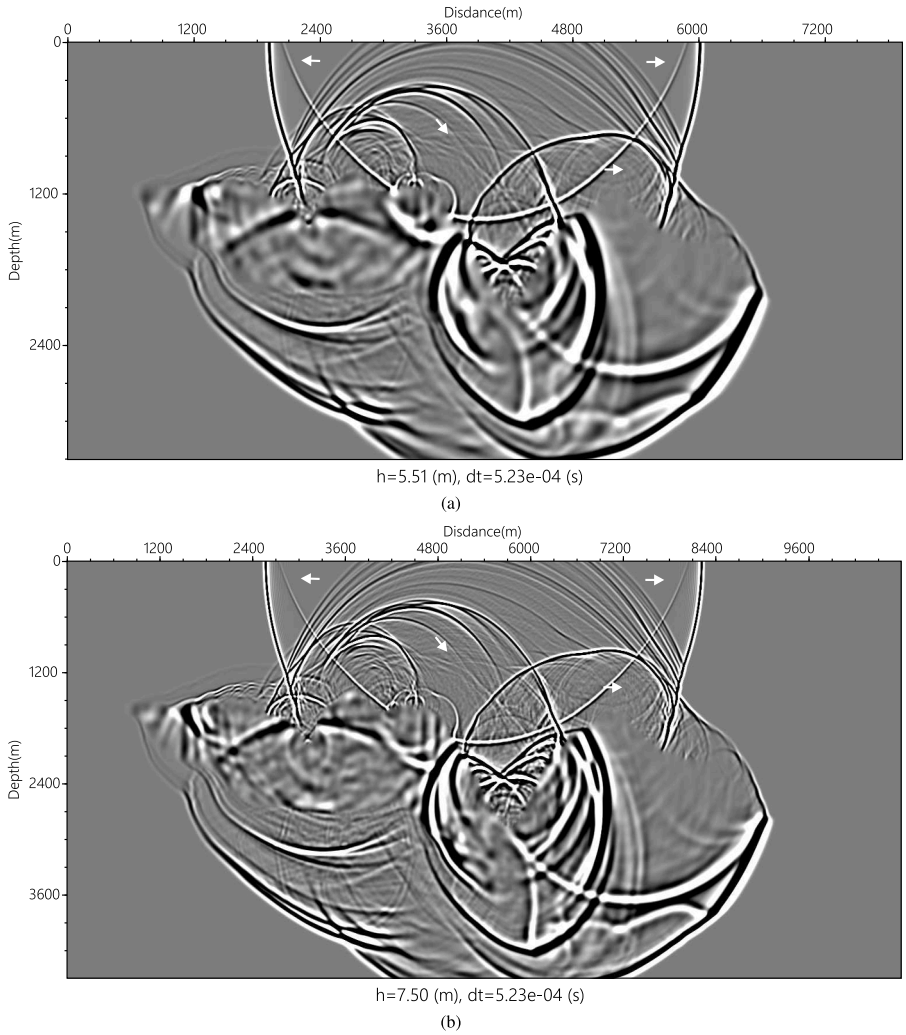

Fig. 11. Snapshots of the 2-D Sigsbee model with different grid spacings h. (a) represents an appropriate grid spacing $h = 5.51$ m from our framework. (b) represents a large grid spacing $h = 7.50$ m.

Table 3
Different grid spacings h we designed for the 2-D model. The benchmark is obtained by our framework.

Cases	M	f_{max} (Hz)	h (m)	τ (s)
Benchmark	8	30*3	5.32	$5.05e{-}04$
1	8	30*3	6.50	$5.05e{-}04$
2	8	30*3	7.50	$5.05e{-}04$

Table 4
Different time steps τ we designed for numerical experiments. The benchmark is obtained by our framework.

Cases	M	f_{max} (Hz)	h (m)	τ (s)
Benckmark	8	30*3	5.32	$5.05e{-}04$
1	8	30*3	5.32	$5.10e{-}04$
2	8	30*3	5.32	$3.00e{-}04$

3. Numerical experiments

3.1. 2-D model with a strong velocity contrast

In this section, we design a 2-D inhomogeneous model to test our framework. The 2-D model has 512×512 grid nodes with the velocities from $v_{min} = 1500$ m/s to $v_{max} = 5500$ m/s. We design a series of experiments to analyze the influence of FD parameters on the numerical simulation. For the convenience of numerical experiments, when setting different grid spacings, we did not interpolate the velocity model, but as a toy experiment with a fixed number of grid nodes. We also ignore the influence of the discrete grid representation on the strong material interfaces (Moczo et al., 2019; Gregor et al., 2020).

Firstly, we set $M = 8$ and $f_{max} = 30 * 3$ Hz for all FD schemes, and a Ricker wavelet is injected as an explosion source. According to the proposed framework, the FD parameters $h = 5.32$ m, $\tau = 5.05e{-}04s$ are automatically calculated as the benchmark. We fix the time step τ, and set different grid spacings h to analyze their numerical results. Table 3 lists the different FD parameters we designed. The snapshots with different h are shown in Fig. 6, and the corresponding dispersion and stability curves are shown in Fig. 7. It can be seen that the snapshot of $h = 5.32$m chosen by the framework has no obvious dispersion phenomenon (Fig. 6(a)), and there is no redundancy in the dispersion and stability curves (Fig. 7(a) and 7(b)). When h increases (Fig. 6(b) and 6(c)), spatial dispersion errors appear in the low-velocity part, because the wavenumber bandwidth no longer satisfies the maximum wavenumber (Figs. 7(c) and 7(e)). Numerical experiments and dispersion analyses prove the effectiveness of our framework in choosing grid spacing h, which ensures that the wavenumber bandwidth is sufficient to deal with the high-wavenumber components of the wavefield.

In the second experiment, we fix the grid spacing h and set different time steps τ to analyze the numerical results. The FD parameters are

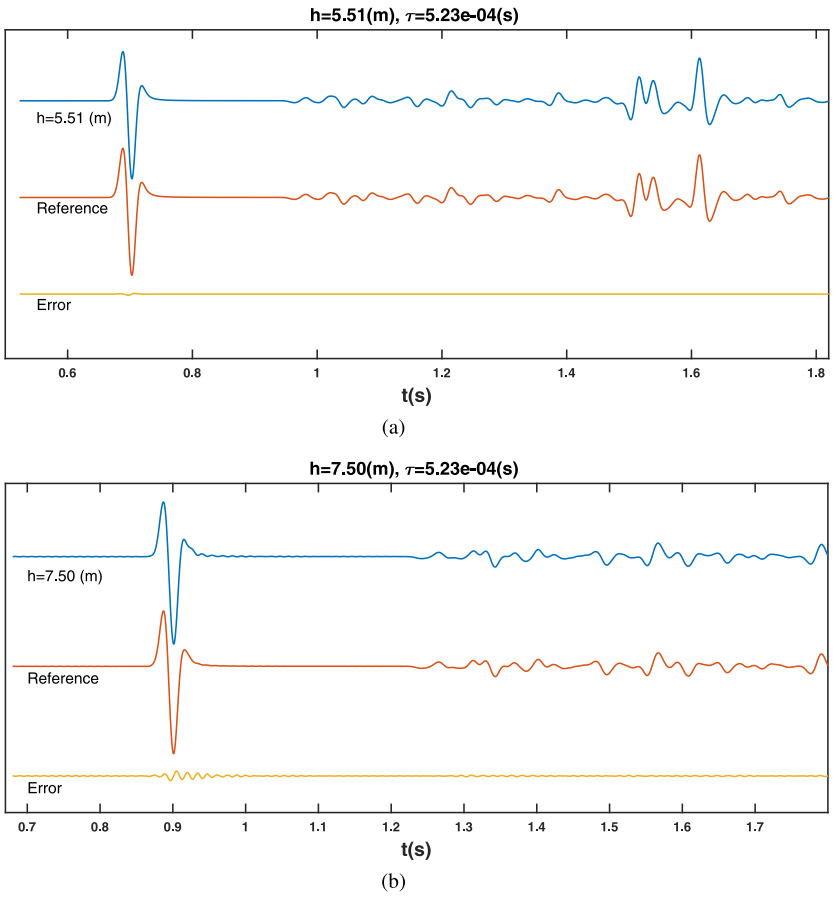

Fig. 12. Seismic waveforms of the 2-D Sigsbee model with different grid spacings h. (a) represents an appropriate grid spacing $h = 5.51$ m from our framework. (b) represents a large grid spacing $h = 7.50$ m.

Table 5
The FD parameters of the 2-D Sigsbee model. The benchmark is obtained by our framework.

Cases	M	f_{max} (Hz)	h (m)	τ (s)
Benckmark	8	30*3	5.51	5.23e−04
1	8	30*3	7.50	5.23e−04

listed in Table 4, and the corresponding results are shown in Fig. 8 and 9. If τ is greater than the optimal value (Case 1 in Table 4), the waves propagation at high-velocity part are unstable(Fig. 8(a)). This result is consistent with the stability analysis (Fig. 9(b)). If τ is less than the optimal value, as shown in Fig. 8(b) and 9(c), there is redundancy in the stability, resulting in unnecessary cost.

3.2. 2-D Sigsbee model

We use a widely referred 2-D Sigsbee velocity model (Paffenholz et al., 2002) to test the validity of our framework in the complex velocity model. The modified 2-D Sigsbee model with velocities from $v_{min} = 1500$ m/s to $v_{max} = 5500$ m/s is shown in Fig. 10, and the positions of source and receiver are also shown in Fig. 10. We set $M = 8$ and $f_{max} = 30 * 3$ Hz for all FD schemes and record the seismic waveform from the receiver. The FD parameters we designed for the 2-D Sigsbee model are listed in Table 5, in which the benchmark is obtained by our framework.

Fig. 11(b) shows that the snapshot of $h = 7.50$ m has obvious dispersion errors in the low-velocity part. This indicates that $h = 7.50$ m is too large, resulting in the FD scheme cannot deal with the maximum wavenumber corresponding to the low-velocity region. Fig. 11(a) shows the snapshot of $h = 5.51$ m, it can be seen that the spatial dispersion errors in the low-velocity part are mitigated. Fig. 12 shows the seismic waveforms of different cases from the receiver. The reference traces come from the temporal and spatial high-order FD scheme (Chen et al., 2020). It can be seen that the case $h = 7.50$ m has obvious relative errors compared with the reference (Fig. 12(b)), while the relative errors are significantly reduced in the case of $h = 5.51$ m (Fig. 12(a)).

4. Discussion

In this paper, we used the second-order scalar wave equation with a regular-grid FD scheme to illustrate the proposed framework. In fact, the proposed framework is universal for the first-order system with the 2-D/3-D staggered-grid FD schemes (Liu and Sen, 2011). The proposed framework can be used as a general method as long as the corresponding dispersion and stability formulas are modified.

The time–space domain FD coefficients are used as the default in this paper, because they consider both the temporal and spatial terms in the dispersion relationship. If the space domain coefficients are adopted, the stability factor s is a constant value. Thus, the stability condition in the framework should be rewritten as:

$$s = \frac{v_{max}\tau}{h}. \tag{22}$$

Eq. (22) indicates that the maximum time step can be obtained directly by

$$\tau = \frac{sh}{v_{max}}. \tag{23}$$

The space domain method is easy to obtain the maximum time step, but the accuracy of the temporal approximation is limited.

The Taylor series expansion method is used to obtain the FD coefficients as an example. However, the Taylor series expansion method satisfies the dispersion relationship in a limited range. The global optimal methods (Zhang and Yao, 2012; Liu, 2013; Wang et al., 2014) or the dispersion-relationship-preserving methods (Ye and Chu, 2005; Liang et al., 2015; Etemadsaeed et al., 2016; Chen et al., 2020) have a wider wavenumber bandwidth for the high-wavenumber components. These wide-bandwidth methods allow the framework to choose larger time step and grid spacing. In addition, the temporal and spatial high-order FD stencils (Tan and Huang, 2014; Ren et al., 2017) are a potential way to obtain a larger time step in the framework, because they have better temporal-approximation accuracy and more relaxed stability condition.

Numerical anisotropy is a ubiquitous phenomenon in the FD methods due to the directionally biased approximations (Sescu and Hixon, 2014; Sescu, 2015). In this paper, the FD dispersion error is calculated along with the propagation angle $\alpha = 0$. If we consider the maximum temporal dispersion error along with the propagation angle $\pi/4$, the FD dispersion error can be rewritten as

$$\begin{aligned}\xi(h, v_{min}, v_{max}) = &\left|\delta(r_a, r_{min}, 0, \beta_{max,v_{min}}) - 1\right| \\ &+ \left|\delta(r_a, r_{min}, \pi/4, \beta_{max,v_{min}}) - 1\right| \\ &+ \left|\delta(r_a, r_{max}, 0, \beta_{max,v_{max}}) - 1\right| \\ &+ \left|\delta(r_a, r_{max}, \pi/4, \beta_{max,v_{max}}) - 1\right|.\end{aligned} \tag{24}$$

Eq. (24) will allow the framework to choose finer parameters, which depends on the approximate accuracy of the FD scheme itself. In essence, multi-directional FD stencils are needed to overcome the numerical anisotropy.

We choose different h for numerical experiments, and do not interpolate the model to make their positions consistent. In the actual model, when we use the framework to determine the FD parameters, we should use the chosen h to interpolate the velocity model. Similarly, the seismic data should be resampled by the chosen time step τ in the reverse time migration or full waveform inversion.

5. Conclusion

We propose a framework to automatically choose the optimal parameters of FD scheme for the seismic wave modeling. The proposed framework determines the FD parameters by considering the dispersion relationship, stability condition and computational cost. For any given velocity model, the framework can choose the optimal FD parameters that satisfy the maximum wavenumber of wavefields and stability condition for all velocities. The chosen parameters lead to the FD scheme that has no redundancy in the wavenumber and stability in the seismic modeling, thus the FD scheme has enough accuracy while ensuring computational efficiency. The framework avoids the trouble of manual choice and provides a better solution for FD scheme.

6. Computer code availability

The reproducible code for this paper is available from GitHub at https://github.com/Guiting-geo.

CRediT authorship contribution statement

Guiting Chen: Code package, Performed the experiments and analyzed the results, Writing – original draft. **Zhenming Peng:** Contributed with the original idea, Analyzed the results, Revised the draft paper. **Yalin Li:** Designed numerical experiments, Discussed the results, Revised the draft paper.

Declaration of competing interest

The authors declare that they have no known competing financial interests or personal relationships that could have appeared to influence the work reported in this paper.

Data availability

The data underlying this article will be shared on reasonable request to the corresponding author.

Acknowledgments

This work is supported by National Natural Science Foundation of China (61775030, 41274127), Sichuan Science and Technology Program, China (2019YJ0167).

References

Amundsen, L., Pedersen, Ø., 2017. Time step n-tupling for wave equations. Geophysics 82 (6), T249–T254.
Chen, J.-B., 2011. A stability formula for Lax-Wendroff methods with fourth-order in time and general-order in space for the scalar wave equation. Geophysics 76 (2), T37–T42.
Chen, G., Wang, Y., Wang, Z., Zhang, S., 2020. Dispersion-relationship-preserving seismic modelling using the cross-rhombus stencil with the finite-difference coefficients solved by an over-determined linear system. Geophys. Prospect. 68 (6), 1771–1792.
Chu, C., Stoffa, P.L., Seif, R., 2009. 3D elastic wave modeling using modified high-order time stepping schemes with improved stability conditions. In: SEG Technical Program Expanded Abstracts 2009.
Dablain, M., 1986. The application of high-order differencing to the scalar wave equation. Geophysics 51 (1), 54–66.
Etemadsaeed, L., Moczo, P., Kristek, J., Ansari, A., Kristekova, M., 2016. A no-cost improved velocity-stress staggered-grid finite-difference scheme for modelling seismic wave propagation. Geophys. J. Int. 207 (1), 481–511.
Etgen, J.T., O' Brien, M.J., 2007. Computational methods for large-scale 3D acoustic finite-difference modeling: A tutorial. Geophysics 72 (5), SM223–SM230.
Fang, J., Chen, H., Zhou, H., Rao, Y., Sun, P., Zhang, J., 2020. Elastic full-waveform inversion based on GPU accelerated temporal fourth-order finite-difference approximation. Comput. Geosci. 135, 104381.
Finkelstein, B., Kastner, R., 2007. Finite difference time domain dispersion reduction schemes. J. Comput. Phys. 221 (1), 422–438.
Gao, Y., Zhang, J., Yao, Z., 2018. Removing the stability limit of the explicit finite-difference scheme with eigenvalue perturbation. Geophysics 83 (6), 1–25.
Gregor, D., Moczo, P., Kristek, J., Mesgouez, A., Lefeuve-Mesgouez, G., Kristekova, M., 2020. Subcell-resolution finite-difference modelling of seismic waves in Biot and JKD poroelastic media. Geophys. J. Int. 224 (2), 760–794.
Le, H., Clapp, R.G., Levin, S.A., Biondi, B., 2020. A pipeline approach for three dimensional time-domain finite-difference multi-parameter waveform inversion on GPUs. Comput. Geosci. 140, 104503.
Liang, W., Wang, Y., Yang, C., 2015. Determining finite difference weights for the acoustic wave equation by a new dispersion-relationship-preserving method. Geophys. Prospect. 63 (1), 11–22.
Lines, L.R., Slawinski, R., Bording, R.P., 1999. A recipe for stability of finite-difference wave-equation computations. Geophysics 64 (3), 967–969.
Liu, Y., 2013. Globally optimal finite-difference schemes based on least squares. Geophysics 78 (4), T113–T132.
Liu, Y., 2019. Acoustic and elastic finite-difference modeling by optimal variable-length spatial operators. Geophysics 85 (2), 1–69.
Liu, G., Liu, Y., Ren, L., Meng, X., 2013. 3D seismic reverse time migration on GPGPU. Comput. Geosci. 59, 17–23.
Liu, Y., Sen, M.K., 2009. A new time–space domain high-order finite-difference method for the acoustic wave equation. J. Comput. Phys. 228 (23), 8779–8806.
Liu, Y., Sen, M.K., 2011. Finite-difference modeling with adaptive variable-length spatial operators. Geophysics 76 (4).
Liu, Y., Sen, M.K., 2011. Scalar wave equation modeling with time-space domain dispersion-relation-based staggered-grid finite-difference schemes. Bull. Seismol. Soc. Am. 101 (101), 141–159.
Liu, Y., Sen, M.K., 2013. Time-space domain dispersion-relation-based finite-difference method with arbitrary even-order accuracy for the 2D acoustic wave equation. J. Comput. Phys. 232 (1), 327–345.
McMechan, G.A., 1983. Migration by extrapolation of time-dependent boundary values. Geophys. Prospect. 31 (3), 413–420.
Moczo, P., Gregor, D., Kristek, J., de la Puente, J., 2019. A discrete representation of material heterogeneity for the finite-difference modelling of seismic wave propagation in a poroelastic medium. Geophys. J. Int. 216 (2), 1072–1099.

Moczo, P., Kristek, J., Gális, M., 2014. The Finite-Difference Modelling of Earthquake Motions: Waves and Ruptures. Cambridge University Press.

Moczo, P., Kristek, J., Galis, M., Chaljub, E., Etienne, V., 2011. 3-D finite-difference, finite-element, discontinuous-Galerkin and spectral-element schemes analysed for their accuracy with respect to P-wave to S-wave speed ratio. Geophys. J. Int. 187 (3), 1645–1667.

Moczo, P., Kristek, J., Halada, L., 2000. 3D fourth-order staggered-grid finite-difference schemes: Stability and grid dispersion. Bull. Seismol. Soc. Am. 90 (3), 587–603.

Mufti, I.R., 1990. Large-scale three-dimensional seismic models and their interpretive significance. Geophysics 55 (9), 1166–1182.

Neumann, J., 1932. Mathematische Grundlagen Der Quantenmechanik. Mathematische Grundlagen der Quantenmechanik.

Paffenholz, J., McLain, B., Zaske, J., Keliher, P.J., 2002. Subsalt multiple attenuation and imaging: Observations from the Sigsbee2B synthetic dataset. In: SEG Technical Program Expanded Abstracts 2002. pp. 2122–2125.

Pan, W., Innanen, K.A., Wang, Y., 2020. SeisElastic2D: An open-source package for multiparameter full-waveform inversion in isotropic-, anisotropic-and visco-elastic media. Comput. Geosci. 145, 104586.

Ren, Z., Li, Z., Liu, Y., Sen, M.K., 2017. Modeling of the acoustic wave equation by staggered-grid finite-difference schemes with high-order temporal and spatial accuracy. Bull. Seismol. Soc. Am. 107 (5), 2160–2182.

Sescu, A., 2015. Numerical anisotropy in finite differencing. Adv. Difference Equ. 2015 (1), 9.

Sescu, A., Hixon, R., 2014. Numerical anisotropy study of a class of compact schemes. J. Sci. Comput. 61 (2), 327–342.

Tan, S., Huang, L., 2014. An efficient finite-difference method with high-order accuracy in both time and space domains for modelling scalar-wave propagation. Geophys. J. Int. 197 (2), 1250–1267.

Virieux, J., Calandra, H., Plessix, R.-E., 2011. A review of the spectral, pseudo-spectral, finite-difference and finite-element modelling techniques for geophysical imaging. Geophys. Prospect. 59 (5), 794–813.

Virieux, J., Operto, S., 2009. An overview of full-waveform inversion in exploration geophysics. Geophysics 74 (6), WCC1–WCC26.

Wang, Y., Liang, W., Nashed, Z., Li, X., Liang, G., Yang, C., 2014. Seismic modeling by optimizing regularized staggered-grid finite-difference operators using a time-space-domain dispersion-relationship-preserving method. Geophysics 79 (5), T277–T285.

Wu, W.-J., Lines, L.R., Lu, H.-X., 1996. Analysis of higher-order, finite-difference schemes in 3-D reverse-time migration. Geophysics 61 (3), 845–856.

Ye, F., Chu, C., 2005. Dispersion-relation-preserving finite difference operators: derivation and application. In: SEG Technical Program Expanded Abstracts 2005. Society of Exploration Geophysicists, pp. 1783–1786.

Zhang, J.-H., Yao, Z.-X., 2012. Optimized finite-difference operator for broadband seismic wave modeling. Geophysics 78 (1), A13–A18.